Journal of Catalysis **186,** 201–213 (1999)
Article ID jcat.1999.2555, available online at http://www.idealibrary.com on IDEAL®

Structure–Activity Correlations on Rh/Al_2O_3 and Rh/TiO_2 Thin Film Model Catalysts after Oxidation and Reduction

Günther Rupprechter,[1] Gernot Seeber,[2] Hans Goller,[3] and Konrad Hayek[4,5]

Institute of Physical Chemistry, Leopold-Franzens-Universität Innsbruck, A-6020 Innsbruck, Austria

Received February 18, 1999; revised May 6, 1999; accepted May 10, 1999

A study of the effect of different supports on the stability and catalytic activity of Rh nanoparticles is only meaningful if the metal particles are perfectly identical in the catalysts to be compared. We have applied epitaxial thin film deposition to produce homogeneous distributions of well-faceted Rh nanocrystals, divided the sample in two, and subsequently supported the metal particles by Al_2O_3 and TiO_2. Three corresponding pairs of Rh/Al_2O_3 and Rh/TiO_2 model catalysts with mean particle sizes of 7.8, 13.3, and 16.7 nm were prepared and activated by different oxidation–reduction treatments at temperatures up to 723 K. The size, morphology, and structure of the metal particles and of the support and the changes upon activation were determined by transmission electron microscopy. Wetting of the support and coalescence of Rh particles were observed to occur upon high-temperature reduction of large (>10 nm) and closely-spaced Rh particles, around 623 K on titania and around 723 K on alumina. Catalysts with smaller Rh particles did not show such pronounced changes. The rate of ring opening of methylcyclobutane at 373 K was measured on the three pairs of Rh/Al_2O_3 and Rh/TiO_2 model catalysts as a function of the reduction temperature after preoxidation at 723 K. Rh/alumina catalysts exhibited maximum activity after reduction at 523 K due to the formation of low-coordinated sites as shown by electron microscopy. The activity of Rh/titania peaked after reduction at 373 K and decreased almost exponentially with T_{red} up to 673 K. In the case of Rh/titania, the changes in particle size and microstructure as observed in the electron microscope can only account for part of the kinetic results. The rapid activity decrease in titania-supported Rh particles with increasing T_{red} is paralleled to an increase in the number of oxygen vacancies and in low-valent Ti cations, on the titania surface. The latter may affect the electric field at the metal–support boundary and thereby reduce the catalytic activity for hydrocarbon reactions. In addition, the decoration of Rh particles by migrating Ti suboxide will account for the diminished activity after reduction at higher temperature.

Key Words: **rhodium nanoparticles; electron microscopy; titanium oxide; aluminium oxide; model catalysts, metal–support interaction; ring opening of methylcyclobutane; neopentane hydrogenolysis.**

1. INTRODUCTION

Supported metal catalysts are generally activated and rejuvenated by cycles of oxidation and reduction at elevated temperature until the system ends up in a steady state characterized by thermally stable metal particles and by high and reproducible reaction rates. Oxidation/reduction cycling not only removes carbonaceous deposits but also may induce significant structural and morphological alterations of the catalyst system, such as faceting, sintering, or redispersion of the metal particles, changes of the metal–oxide boundary, alloying, and others. The type of pretreatment has, therefore, a major influence on the performance of the catalyst; e.g., it is well known that a hydrogen reduction at 773 K and above may result in a diminished catalytic activity of noble metals supported by reducible oxides (1, 2). Consequently, well-defined reduction states are an indispensable condition in a study of structure–activity correlations of hydrocarbon reactions. In this communication, we will analyze the structure and morphology of Rh/Al_2O_3 and Rh/TiO_2 catalysts in various reduction states and compare their activities in a structure-sensitive hydrocarbon reaction. It will be shown that, depending on the metal loading, hydrogen reduction may induce significant structural changes like particle spreading, coalescence and redispersion, with pronounced influence on the catalytic activity.

A meaningful study of support effects anticipates that the metal particles are identical in the corresponding Rh/Al_2O_3 and Rh/TiO_2 catalysts. This can be perfectly realized by using epitaxially grown thin film model catalysts. Their advantages to studies of microstructural changes of noble metal particles have been listed in previous articles (3–7). Well-faceted Rh nanocrystals are grown epitaxially on a large area NaCl support before one-half of the Rh/NaCl sample is covered with Al_2O_3 while the other half is backed with

[1] Present address: Fritz-Haber-Institut der Max-Planck-Gesellschaft, Chemical Physics Department, Faradayweg 4-6, D-14195 Berlin, Germany, E-mail: rupprechter@fhi-berlin.mpg.de.

[2] Present address: Institute of Analytical Chemistry and Radiochemistry, Leopold-Franzens-Universität Innsbruck, Austria.

[3] Present address: Sony Co., Salzburg, Austria.

[4] E-mail: Konrad.Hayek@uibk.ac.at.

[5] To whom correspondence should be addressed.

0021-9517/99 $30.00

TiO_2. The model catalyst films are finally removed from the NaCl substrate by flotation. The preparation of Rh particles for both Al_2O_3- and TiO_2-supported model catalysts *in a single step* prevents any differences in particle size, shape, and surface structure which could occur if the samples were prepared in separate experiments. Due to the regular polyhedral habit of the epitaxial Rh nanocrystals (half octahedra, rectangular pyramids, etc.), these particles provide a definite initial state, allowing an easier detection and a better understanding of the alterations during the subsequent activation and reaction. Due to their small thickness of about 25 nm, thin film model catalysts are particularly suited for characterization by electron microscopy and electron diffraction. Furthermore, metal nanocrystals grown on large area NaCl substrates (100 cm^2) provide sufficient surface area for kinetic measurements in a microreactor (8).

In a recent study (3), alumina-supported Rh nanocrystals (3–10 nm in size) were subjected to comparatively moderate activating treatments, i.e., to oxidation and reduction at atmospheric pressure at 723 K and below. Structural changes of individual Rh particles of different crystallographic habit were recorded by high-resolution electron microscopy (HREM), selected area electron diffraction (SAED), and weak-beam dark-field (WBDF) imaging. Oxidation up to 723 K resulted in the growth of an epitaxial oxide layer around an intact metal core. Upon a subsequent low-temperature hydrogen treatment (473–523 K), we observed the reduction of the rhodium oxide shell starting from the outer particle surface and the formation of polycrystalline metal aggregates and metal–oxide–metal sandwich structures besides fully reduced nanocrystals. Reduction at higher temperature, however, up to 723 K, led to a complete recrystallization of all particles into nanocrystals with low-index surfaces.

The regular Rh nanocrystals described in Ref. (3) had been produced by physical vapour deposition onto atomically flat NaCl (001) substrate surfaces and were thereafter embedded in an amorphous alumina support. Random nucleation of the metal on the smooth NaCl surface had resulted in isolated, well-separated particles with interparticle distances of about tens of nanometers. In this case, wetting or sintering phenomena as a result of hydrogen reduction were not observed up to 723 K. On the contrary, on "rougher" (less homogeneous) supports, like NaCl films of small grain size, the higher nucleation probability along NaCl steps and grain boundaries gave rise to smaller but more closely spaced metal particles in the respective areas of the resulting catalyst film. Upon reduction around 673 K, it was observed that these closely neighboured particles (average size 5 nm) underwent sintering and coalescence quite easily while the separated particles in the "flat" catalyst regions were still unaffected. Consequently, we can assume that an increase of the metal loading, reducing the interparticle distance, will presumably induce sintering and coalescence upon reduction in the flat regions as well, and hence permit a study of the influence of these phenomena on the catalytic activity. Both sintering and coalescence are determined by the interfacial energy between metal and oxide and will depend strongly on the properties of the support.

These considerations led us to prepare a series of larger (and less distant) Rh nanocrystals than those discussed in Ref. (3), to support them on alumina and titania, and to try to correlate their structure and activity in various states of reduction. For a study of reduction temperatures lower than 523 K (as generally applied), a test reaction proceeding at lower temperature was needed. The ring-opening reaction of methylcyclobutane (MCB) with hydrogen is structure sensitive (9, 10) and occurs easily at 373 K and below. It is therefore well suited to measure the effect of a reduction between 373 and 673 K. The influence of reduction temperatures above 473 K can be tested in a number of well-investigated structure-sensitive reactions, e.g., in the hydrogenolysis of neopentane.

2. METHODS

Three pairs of corresponding Rh/Al_2O_3 and Rh/TiO_2 model catalysts were prepared, each pair containing Rh particles of identical size and shape. The metal particles were characterized by various electron microscopy techniques as described below.

2.1. *Catalyst Preparation*

Large area NaCl substrates (100 cm^2) were prepared *in situ* by vacuum deposition onto polished Cu sheets at 360 K (rate, 10 nm min^{-1}; thickness, 100 nm). The resulting NaCl films consisted of grains with (001) surfaces a few microns in size.

Three different Rh thin films, with a nominal (theoretical) thickness of 0.8, 2.4, and 4.2 nm, were grown by electron beam evaporation on NaCl films at a substrate temperature of 598 K and a base pressure of 1×10^{-7} mbar (1 mbar = 100 Pa; growth rate: 0.1 nm min^{-1}). A nominal film thickness of 0.8, 2.4, and 4.2 nm translates into a mean Rh particle size of 7.8, 13.3, and 16.7 nm, respectively. After the films were cooled to room temperature *in vacuo*, one-half of each island-stage Rh film (area $\approx$40 cm^2) was backed with a support of 25 nm of Al_2O_3 by reactive evaporation of Al metal in 10^{-4} mbar of oxygen (rate: 1 nm min^{-1}). The other half was subsequently coated with a titania film of the same thickness by reactive evaporation of titanium in oxygen. A systematic study of the influence of preparation parameters on the properties of epitaxially grown thin film model catalysts has been given previously (5). In the as-prepared state, the supporting oxide films were amorphous. The amorphous alumina film was thermally stable, but it crystallized to γ-alumina under high-intensity electron beam irradiation (3). The titania film crystallized into

the anatas structure upon heating above 573 K, but it was not affected by electron irradiation in the microscope.

Small parts of the six so-obtained Rh/oxide films were removed from the NaCl substrates by flotation, rinsed thoroughly in water, and mounted on 3 mm Ø gold grids for electron microscopy examination. The remaining films (area, 38 cm^2) were used for catalytic measurements after their mechanical stability was increased by a second oxide coating on top of the support. The thicker metal/oxide films were also floated in water and washed several times and the resulting small flakes were transferred to the reactor cell where they were held between two glass wool plugs.

2.2. Catalyst Activation by Oxidation and Reduction

The model catalyst films and the corresponding electron microscopy sample grids were placed together in the glass microreactor for activation and subsequent reaction studies. Oxidation and reduction treatments were performed under 1 bar of oxygen or hydrogen, respectively, at temperatures between 323 and 723 K for periods of 30 or 120 min. After every step, the system was evacuated and purged with helium several times. Kinetic data were taken after every oxidation/reduction cycle. After an activation process and/or after a reaction, some of the TEM samples were removed from the system and inspected in the electron microscope.

2.3. Electron Microscopy

Conventional transmission electron microscopy (CTEM), selected area electron diffraction (SAED), and weak-beam dark-field (WBDF) imaging were applied to determine the morphology and the microstructure of the model catalysts (Zeiss EM 10C and JEOL 100C operated at 100 kV). Some samples were also imaged at lattice resolution in a JEOL 4000EX operated at 400 kV as described in detail in (3). Digital image processing was utilized for contrast enhancement of the CTEM micrographs and for the determination of the mean particle diameter, the particle number density, and the metal surface area of the catalysts (software Image ProPlus by Media Cybernetics and NIH Image by Wayne Rasband). Elemental maps and profiles were aquired using energy-dispersive X-ray analysis (EDX) to check the composition of the films (JEOL 200CX; Emispec Systems, Si-detector from Kevex).

2.4. Kinetic Measurements

Kinetic studies of the hydrogenolysis of methylcyclobutane (MCB) were performed in the computer-controlled microreactor system described in (8). It is a circulated batch reactor with a 16-ml volume and particularly suited to study the small amounts of catalyst available by thin film deposition. The reaction products were analyzed by gas chromatography using a flame ionization detector, and conversion vs time plots were acquired after every oxygen/hydrogen treatment.

As known from our previous studies (10) and also from results of other authors (9, 11, 12), the rate of the MCB ring-opening reaction depends strongly on the hydrogen partial pressure and it generally passes a maximum as a function of the latter. In these experiments, at 373 K and an MCB pressure of 5 mbar, the highest reaction rates were obtained at a P_{H_2} of 100 mbar with helium added up to 1 atm. The hydrogen pressure dependence of the reaction rates was not changed significantly by the applied catalyst activation treatments. The main variable in our experiments, the temperature of hydrogen reduction, was increased in steps from 373 to 673 K with the reduction time being either 30 or 120 min.

From the conversion vs time plots, the *initial* catalytic activity was determined. The measured activities were converted into initial turnover frequencies by relating them to the metal surface area calculated from electron micrographs of the catalysts (the particle projections in the microscopic images correspond, in general, to the base planes of the metal particles). As will be shown below, the effective metal surface area is predominantly determined by the state of oxidation or reduction and the particle size, and also by the encapsulation of the metal by the support.

The study of the methylcyclobutane ring-opening reaction was complemented by measurements of neopentane hydrogenolysis on the same catalysts. This is a well-investigated structure-sensitive reaction and a useful test for comparison of the measured activities with data from the literature. Initial activities were determined at a reaction temperature of 473 K. The partial pressure of neopentane was 5 mbar, and the hydrogen pressure was varied between 50 and 800 mbar with helium added to 900 mbar. In this case, the reduction temperature could be varied between 473 and 673 K.

3. RESULTS

3.1. Particle Oxidation

As reported previously (3, 5, 13), epitaxially grown Rh nanocrystals exhibit a variety of polyhedral shapes which can be identified by HREM and weak-beam dark-field imaging. Figure 1a shows a bright-field micrograph of the "7.8-nm" Rh/Al_2O_3 model catalyst (mean particle size, 7.8 nm; metal coverage, 17%; nominal Rh film thickness, 0.8 nm), and the corresponding WBDF image is presented in Fig. 1b. The Rh particles were identical in the 7.8-nm Rh/TiO_2 catalyst due to the parallel preparation of both systems (cf. Section 2.1). WBDF micrographs image the thickness contours of the particles, and from the fringe structure and fringe spacings the particle shape and height can be deduced (5, 14, 15). In general, half-octahedral particles

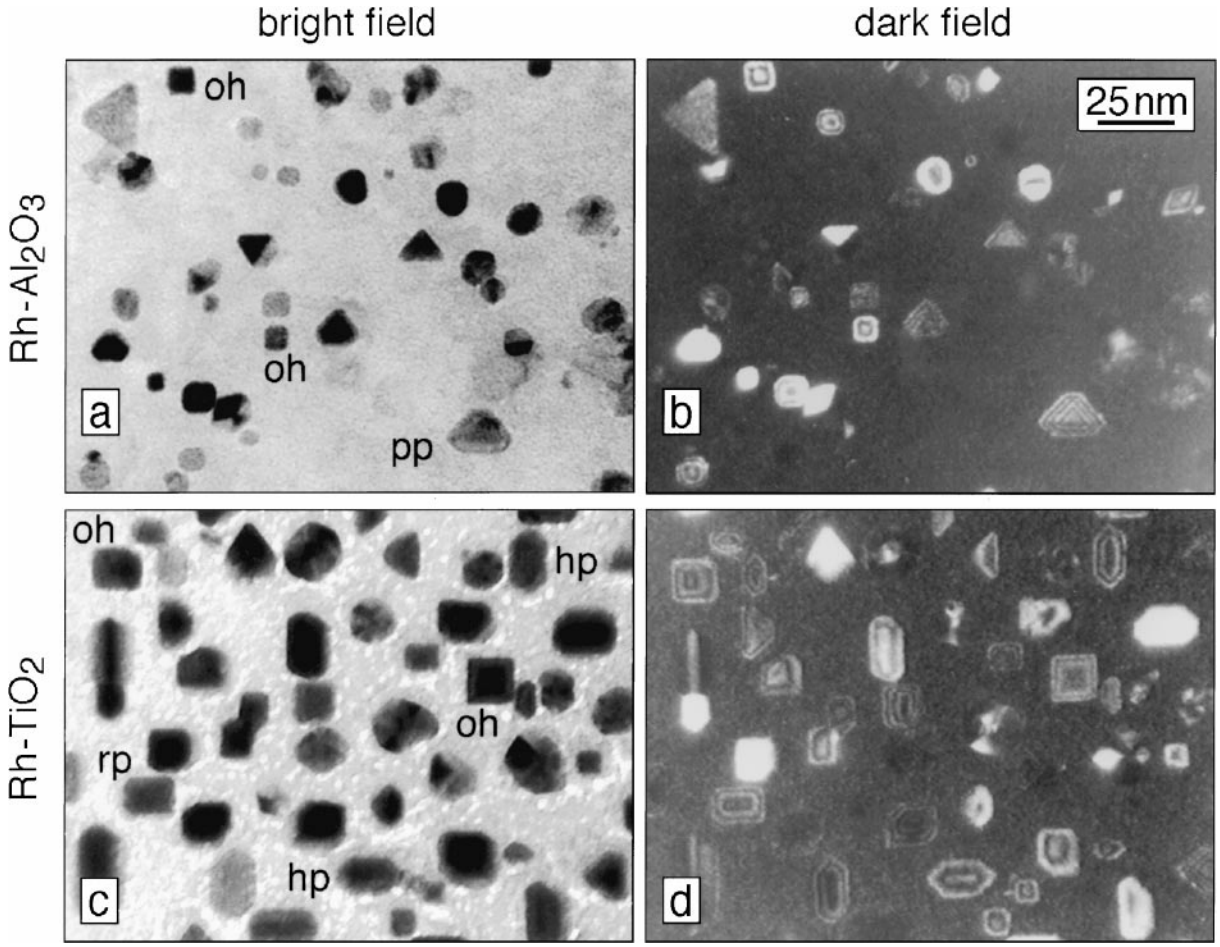

FIG. 1. Bright field electron micrographs of oxide-supported Rh nanoparticles: (a) Rh on alumina (mean particle size, 7.8 nm) and (c) Rh on titania (mean particle size, 13.3 nm). The corresponding (200) weak-beam dark-field images are shown in (b) and (d). A few polyhedral nanocrystals are indicated: Half-octahedron (oh), rectangular pyramid (rp), pseudopentagonal pyramid (pp), and hexagonal pyramid (hp).

(with square outlines; marked "oh" in Fig. 1) or closely related habits like rectangular pyramids and pseudopentagonal pyramids (marked "rp" and "pp" in Fig. 1) are predominant which all expose (001) base planes to the reactant gas. A half-octahedral Rh particle exhibits an angle of 55° between its base and side facets, and its height is therefore 71% of its diameter (for example, an 8-nm diameter particle has a height of 5.7 nm—in the case of an untruncated top). A model catalyst of higher metal loading is presented in Figs. 1c and 1d. They show bright- and dark-field images of the 13.3-nm Rh/TiO_2 catalyst in the as-prepared state (metal coverage, 43%; nominal Rh film thickness, 2.4 nm). HREM micrographs of two Rh nanocrystals are presented in Fig. 2. While a *perfect* rectangular pyramid exhibits a (001) base plane and four {111} side faces, the rectangular pyramid shown in Fig. 2a has one corner truncated by a small {110} plane. If more corners are truncated, hexagonal particles can be observed, such as that in Fig. 2b, in this case, with a (001) base plane, two {111} and four {110} side facets (for details and schematic models, see (3, 6, 15)). Some hexagonal pyramids can be clearly identified in Figs. 1c and 1d (marked "hp"). An as-grown 16.7-nm Rh/TiO_2 catalyst (metal coverage, 61%; nominal Rh film thickness, 4.2 nm) is shown in Fig. 3a. It consists of larger and even more closely spaced metal particles, and many of them have truncated (rounded) corners. Some Rh particles are coalesced or are polycrystals, but regular particle shapes with distinct facets are also present. The number of Rh particles per thin film catalyst area was almost constant on all three pairs of catalysts because a NaCl substrate temperature of 598 K was used in all experiments, resulting in identical nucleation densities of Rh on NaCl (around 3×10^{11} cm^{-2} (5)). Therefore, the higher metal loadings led to an increase in particle size and a decrease in the interparticle distance.

Upon exposure to 1 bar of oxygen up to 723 K, the Rh particles in all catalysts underwent almost identical changes independent of support and particle size. The changes occurring on small (~5 nm) Rh particles were reported in detail in Ref. (3). They can be summarized as the formation

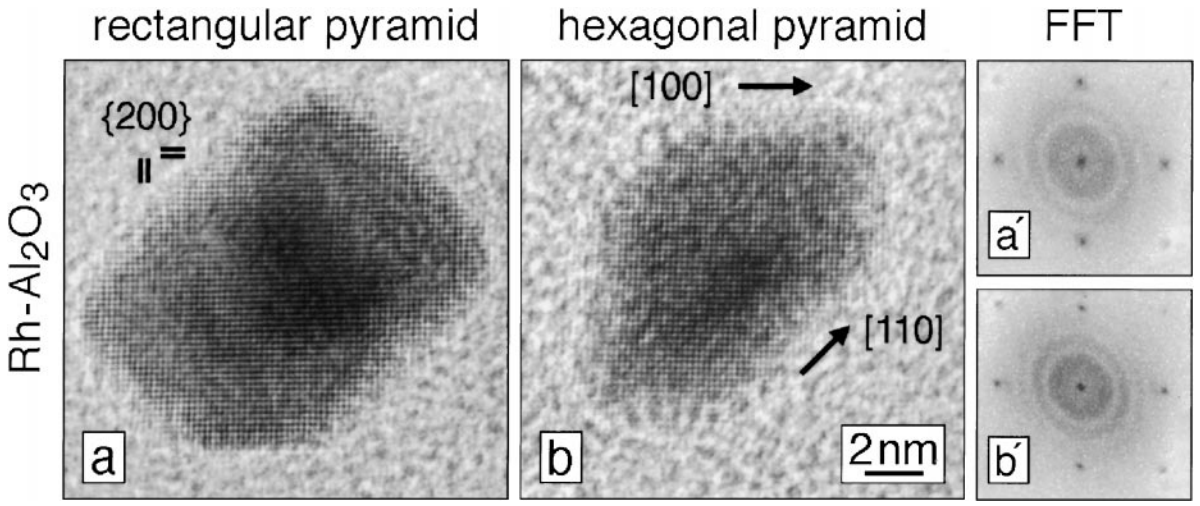

FIG. 2. High-resolution electron micrographs of polyhedral Rh nanoparticles on alumina in (001) zone axis orientation: (a) rectangular pyramid with (001) base, four {111} side facets, and one small {110} truncation, and (b) hexagonal pyramid with a (001) base, two {111}, and four {110} side facets. (a′) and (b′) are the corresponding fast Fourier transforms.

of a thin surface oxide after oxygen exposure up to 673 K, and of an epitaxially growing Rh_2O_3 shell upon oxidation at higher temperature. Figures 3b and 3c depict the changes of the 16.7-nm Rh/TiO_2 catalyst. After a 673 K oxidation for 120 min, the particles appeared unchanged under medium magnification (Fig. 3b), but a surface oxide layer could be visualized by HREM (3). Oxygen exposure at 723 K for 120 min induced the formation of a Rh_2O_3 shell and was accompanied by a volume increase of approximately 30% but leaves the metal cores intact (Fig. 3c). In Fig. 3c it is also seen that the volume increase may lead to a contact of adjoining particles, but not to merging or coalescence. The overlap of oxide and metal and the difficulty to separate Rh–oxide and metal diffraction spots prevented well-resolved WBDF thickness contours, but the overall particle shape was clearly maintained.

In the as-prepared state, the supporting oxide films were amorphous. According to SAED, heating above 573 K induced a crystallization of the amorphous titania support into the anatas modification, resulting in minor changes of the support contrast, but obviously not affecting the metal particles. The alumina film remained amorphous up to 800 K, but it crystallized to γ-alumina under repeated high-intensity electron beam irradiation, as shown by HREM and SAED (3). The titania film was not affected by electron irradiation in the microscope.

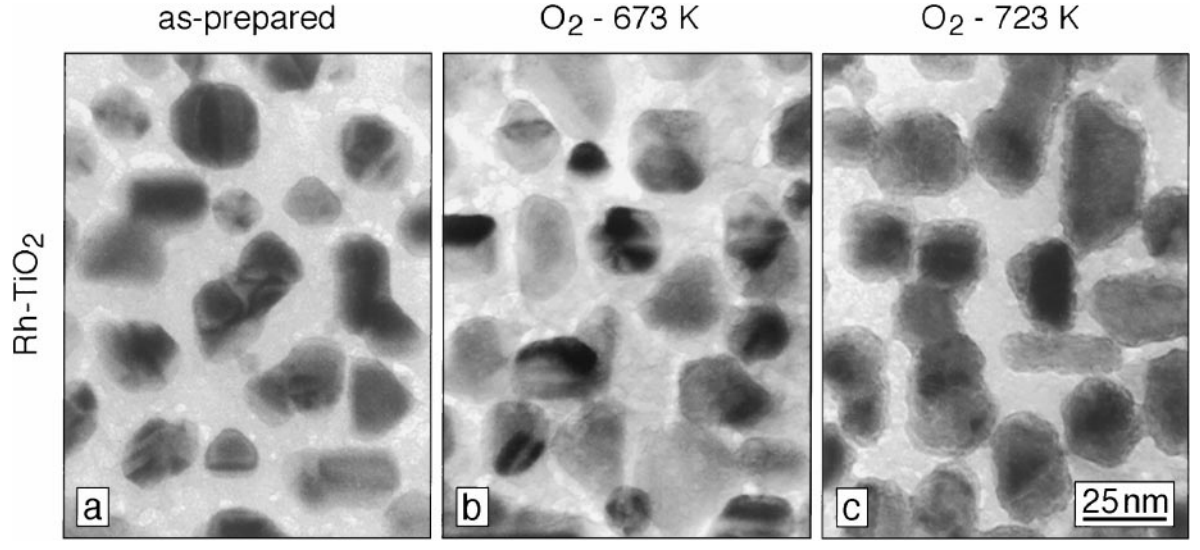

FIG. 3. Effect of successive oxidation on a Rh/titania catalyst (mean particle size, 16.7 nm): (a) as-prepared, (b) after oxidation at 673 K (120 min), and (c) after oxidation at 723 K (120 min).

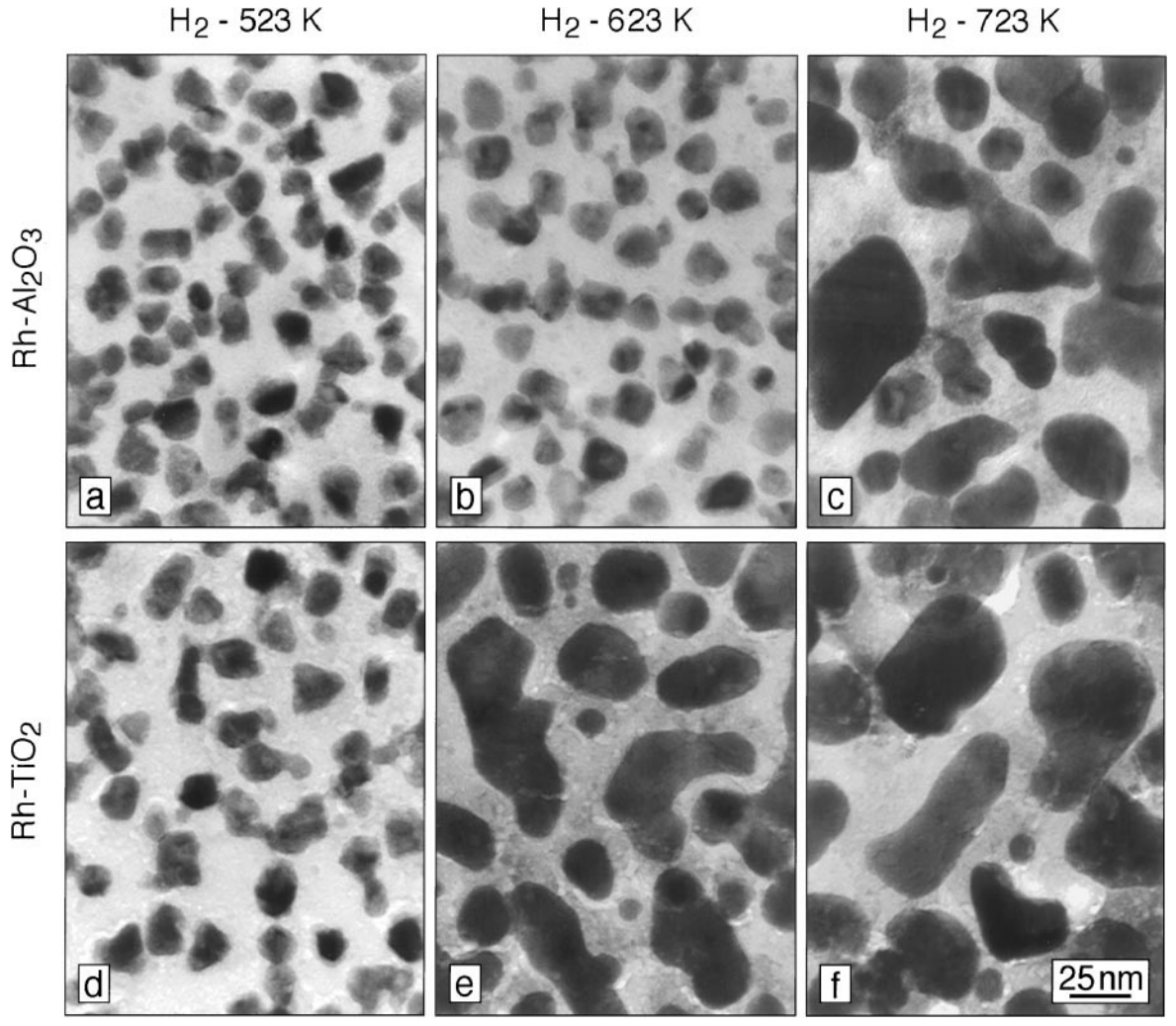

FIG. 4. Effect of successive reduction on preoxidized Rh/Al_2O_3 (upper row) and Rh/TiO_2 (lower row) catalysts (average Rh particle size, 13.3 nm): Oxidation at 723 K (120 min) was followed by reduction (30 min) at 523 K (a, d), at 623 K (b, e), and at 723 K (c, f).

3.2. Reduction after Oxidation

The oxidized model catalysts were subsequently subjected to reduction in H_2 at various temperatures (Fig. 4). The effect of a low-temperature reduction up to 573 K ("LTR") on particles preoxidized at 723 K was independent of the particle size or metal loading. After LTR, most particles exhibited rounded or irregular outlines and only a few particles had maintained distinct edges. SAED indicated a complete reduction of the oxide shell to Rh metal, but HREM and WBDF images revealed a considerable number of polycrystalline aggregates (3). A similar effect has been observed by Datye *et al.* on Rh/SiO_2 (16, 17) and by Bernal *et al.* on Rh/TiO_2 (18), indicating that a reduction temperature around 523 K may be too low for a perfect recrystallisation of oxidized Rh particles into the habit of the original (single-crystal) particles. Irregular and polycrystalline Rh particles have disordered surface structures which are of importance with respect to their catalytic activity, as will be outlined below.

After reduction at higher temperature, the catalysts of low metal loading (small particles, large interparticle distance) and those of high metal loading (large and closely spaced particles) behaved differently. After a high-temperature reduction ("HTR") up to 723 K for 30 min, the small and well-separated particles ($d = 7.8$ nm) on *either* support exhibited rounded profiles on CTEM images. HREM micrographs showed single-crystalline Rh particles only, proving a complete recrystallisation into nanocrystals (3). This was further corroborated by the WBDF thickness fringes of the particles, indicating that the original pyramidal shapes were regained. Only in areas of (former) NaCl grain boundaries, with particles closely spaced even at low metal loading, coalescence was observed.

However, rather unexpected changes occurred upon HTR of the catalysts of higher loading (Rh on Al_2O_3 and

on TiO_2 with $d = 13.3$ and 16.7 nm, pictured in Figs. 1c and 3c). As mentioned above, a reduction up to 573 K resulted only in minor alterations similar to those observed on small particles, but a further increase of the reduction temperature provoked severe coalescence and spreading of Rh particles on alumina (starting around 723 K) and on titania (starting already around 623 K). Figures 4a and 4d show the 13.3-nm Rh/Al_2O_3 catalyst and the 13.3-nm Rh/titania catalyst after a LTR at 523 K, resulting in separated oxide-free particles (metal coverage ca. 45%). Reduction at 623 K of Rh/Al_2O_3 induces a further rounding of particle corners (Fig. 4b). Upon subsequent reduction at 723 K, the metal particles start to merge and to spread over the support surface (Fig. 4c, metal coverage ca. 55%). The reduction of the 13.3-nm Rh/TiO_2 catalyst induces similar sintering and spreading phenomena, but already at a much lower temperature. After reduction at 623 K, particle coalescence has occurred and most particles have lost their original shape while the overall metal coverage of the surface has seemingly increased (Fig. 4e, metal coverage ca. 52%). As indicated by electron diffraction and HREM, it is indeed *metallic* Rh that wets the titania surface and spreads over the TiO_x support. The WBDF thickness fringes indicated that the coalesced particles are rather flat patches up to 5-nm thick. Also, the TEM contrast suggests that the *average* mass thickness is the same and only the distribution along the surface has changed. This appearance remains almost unchanged upon a further increase of the reduction temperature to 723 K (Fig. 4f, metal coverage ca. 55%). It has been reported that upon high-temperature reduction gold from a TEM grid may become mobile and alloy with the specimen (19). We have therefore acquired elemental maps and profiles using energy-dispersive X-ray analysis, but no accumulation of Au was evident in the Rh islands.

Bernal *et al.* (18) have shown that metal decoration and sintering in a Rh/TiO_2 catalyst upon reduction at 773 K and higher may be connected to a change in the support surface (amorphisation). As mentioned before, our titania film crystallized into the anatas structure upon heating above 573 K, while the alumina film remained amorphous. The difference in the ability of the Rh particles to spread on the support at elevated reduction temperature may therefore be due to the fact that crystalline TiO_2 is "smooth" while amorphous Al_2O_3 is "rough". However, when the support crystallization was incomplete, spreading of Rh particles supported on crystalline and amorphous titania or alumina could be observed simultaneously. A significant influence of the support morphology was therefore not detected. As will be discussed below, the different spreading behaviour more likely reflects the influence of a high-temperature reduction on the oxidation state of the support.

3.3. Cycles of Oxidation and Reduction

After a 723 K reduction of the preoxidized 13.3-nm catalysts, the Rh metal film covers about 55% of the surface of either support (Figs. 4c and 4f). A second oxygen exposure at 723 K for 120 min results in an extended oxidation to Rh_2O_3, together with a volume increase and an increase of the apparent support surface coverage to about 60% (Fig. 5a). The retained metal cores are surrounded by large flat oxide areas and these are linked by bridges of rhodium oxide. A subsequent low-temperature reduction at 523 K (30 min) of Rh/Al_2O_3 and of Rh/TiO_2 induces a breakup of these oxide bridges, and a retraction of the metal into clusters of ~20-nm size, somewhat larger than the original Rh particles of 13.3-nm mean size and now with a rounded pyramidal shape (Fig. 5b, metal coverage ca. 50%, to be compared to Fig. 1c). In between these large clusters, a

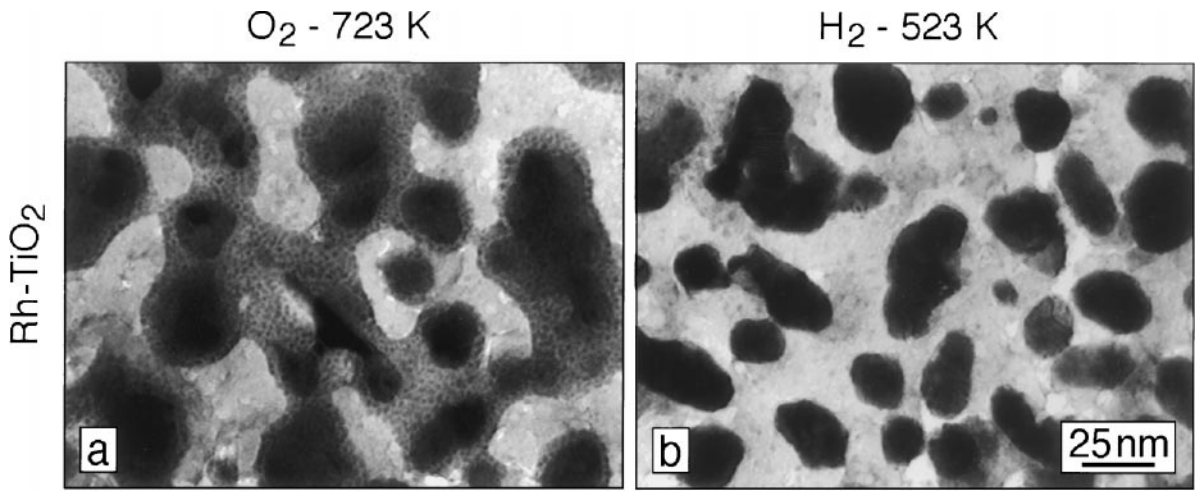

FIG. 5. Structural changes of the 13.3-nm Rh/titania catalyst shown after a high-temperature reduction in Fig. 4f, after an additional oxidation at 723 K (a) and a subsequent low-temperature reduction at 523 K (b).

limited number of much smaller Rh particles (<2 nm in size) are also observed in both cases, as a result of redispersion leading to a bimodal particle distribution. Rh particles of this type appear only after LTR of an extensively oxidized catalyst and are probably identical to those observed by Wang and Schmidt (20) on Rh/SiO_2 and Rh/Al_2O_3 model catalysts under similar conditions. After another HTR, at 623 K of Rh/TiO_2 and at 723 K of Rh/Al_2O_3, the already described phenomena, spreading and coalescence, are again observed. A consecutive oxidation/LTR will then result in the same particle distribution as before. This cycle of oxidation and reduction may be repeated several times, leading to an identical state of recovery after every LTR. An almost identical behaviour was observed on the two 16.7-nm catalysts, while on the 7.8-nm catalysts no coalescence and spreading was detected, even after repeated cycles of oxidation and reduction.

3.4. Kinetic Measurements

Reaction of methylcyclobutane and hydrogen at 373 K. Figure 6 illustrates the effect of the reduction temperature on the MCB ring-opening rate on 7.8-nm Rh/Al_2O_3 and 7.8-nm Rh/TiO_2. The conversion is plotted vs time after reduction at 373 and 523 K (the temperature of preoxidation was 723 K in both cases). A reduction at 373 K is not sufficient to activate Rh on Al_2O_3, but a high and reproducible activity is measured upon reduction between 523 and 573 K, like on most alumina-supported platinum metals. However, a reduction at 373 K (i.e., at the reaction temperature) yields the highest activity of Rh on TiO_2, but in this case the reaction rate decreases with increasing T_{red}.

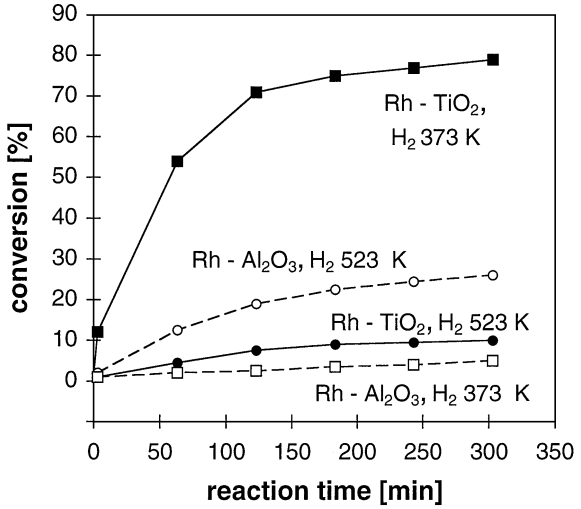

FIG. 6. Conversion vs time plot of 7.8-nm Rh/titania (full lines) and 7.8-nm Rh/alumina (dashed lines) after 30 min of hydrogen reduction at 373 K (■) and 523 K (●). Reaction conditions: 5 mbar methylcyclobutane; 100 mbar hydrogen; reaction temperature 373 K; preoxidation at 723 K.

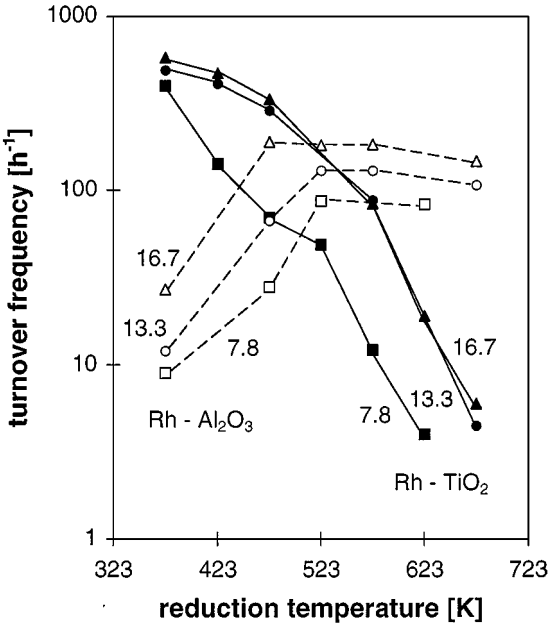

FIG. 7. Dependence of the initial ring-opening activity of Rh/titania (full lines) and Rh/alumina (dashed lines) on the reduction temperature. The mean size of the Rh particles was 7.8 (■), 13.3 (●), and 16.7 (▲) nm. Reaction conditions: 5 mbar methylcyclobutane; 100 mbar hydrogen; reaction temperature 373 K; preoxidation at 723 K.

At this point, the selectivity of the reaction, i.e., the ratio of isopentane and *n*-pentane in the products, should be discussed. On one hand, in agreement with previous investigations of MCB ring opening on noble metal/oxide systems (9, 10, 12), the selectivity was found to depend on the hydrogen pressure. On the other hand, its dependence on particle size was rather small, probably due to the fact that the particle dimensions used in this work were already quite large (>4 nm). To rule out the effect of hydrogen pressure, the reaction rates were always studied at a constant P_{H_2} near the experimentally observed rate maximum (which was not shifted due to reduction). In this case, the selectivity was nearly the same in all the reactions. It varied slightly with the conversion (reaction time), but under steady state conditions an isopentane/*n*-pentane ratio of 4.5 ± 0.5 was always measured. The selectivity did, however, not change as a function of the reduction treatment. This indicates that the number of active sites is reduced by the effects discussed later on (oxygen vacancies and decoration), but that the nature of the remaining active sites is not changed appreciably by the hydrogen treatments.

The initial turnover frequencies of the reaction as a function of the reduction temperature are plotted in Fig. 7 and the results are also summarized in Table 1. The TOF was calculated based on the metal surface areas determined by digital image analysis of micrographs showing the different reduction states (cf., for example, Fig. 4f representing the 13.3-nm catalysts after a 723 K reduction). Although the

changes in the metal coverage were comparatively small (e.g., from about 43 to 55% for the 13.3-nm catalysts), dramatic activity changes were observed.

While there is fair agreement between the initial TOF values of the 13.3-nm and 16.7-nm TiO_2-supported catalysts (Fig. 7), the turnover rates of these catalysts differ markedly from those of the smaller titania-supported particles (7.8-nm catalyst). All three Rh/TiO_2 catalysts exhibit the highest activity after reduction at 373 K (reduction below 373 K does not completely decompose Rh_2O_3), but on the small 7.8-nm particles the TOF decreases almost exponentially with T_{red} up to 623 K (the low conversions allow only estimates for reduction above 623 K). The activity of the larger particles decreases less drastically upon reduction, but it also diminishes upon HTR above 673 K.

On the contrary, the Rh/Al_2O_3 catalysts are inactive after reduction below 373 K. Upon reduction between 373 and 523 K, the activity increases to a flat maximum, followed by a slight decrease upon reduction up to 673 K. Finally, after reduction at 673 K, the activity of a Rh/Al_2O_3 catalyst is about 25 times higher than that of the corresponding Rh/TiO_2 sample. After reduction at 523 K and above, the agreement between the TOFs of the three alumina-supported catalysts was better than that at lower reduction temperatures. It seems that on alumina the smaller particles need higher reduction temperatures for activation, probably due to an effectively stronger preoxidation of small particles.

Reaction of neopentane with hydrogen at 473 K. A meaningful hydrogen reduction must always occur at or above the temperature of the subsequent reaction under study. Therefore, only a smaller range of reduction temperatures, between 473 and 723 K, was available for the investigation of the hydrogenolysis of neopentane, and some representative TOFs are presented in Table 2. The neopentane conversion was nearly independent of the particle size, and the differences between Rh/Al_2O_3 and Rh/TiO_2 after LTR or HTR were smaller than those in the MCB conversion. The activity of all catalysts was high when a preoxidation at 723 K was followed by a LTR at 523 K. A subsequent HTR resulted in an activity decrease, in agreement with reports in the literature (21, 22). After a LTR (e.g., in particular, after reduction at 523 K), the activity of Rh/titania was somewhat higher than that of Rh/alumina, but the decrease with T_{red} was more pronounced on titania. As shown previously (3), the activity decrease upon HTR of alumina-supported Rh can be correlated with a change of the surface structure of the Rh particles, i.e., a decrease of the roughness due to the formation of low-index facets.

TABLE 1

Initial Turnover Frequencies (h^{-1}) of Methylcyclobutane Hydrogenolysis on Rh/Al_2O_3 and Rh/TiO_2 Thin Film Model Catalysts after Preoxidation at 723 K Followed by Reduction at Various Temperatures

	Reduction temperature						
	373 K	423 K	473 K	523 K	573 K	623 K	673 K
7.8-nm Rh/Al_2O_3	9		28	87		84	
7.8-nm Rh/TiO_2	397	143	70	49	12	4	
13.3-nm Rh/Al_2O_3	12		67	130	130		108
13.3-nm Rh/TiO_2	489	410	288		88		5
16.7-nm Rh/Al_2O_3	27		190	182	184		148
16.7-nm Rh/TiO_2	577	470	334		84	19	6

Note. Reaction conditions: 5 mbar MCB; 100 mbar hydrogen; 900 mbar He. Reaction temperature: 373 K. Preoxidation at 723 K.

TABLE 2

Initial Turnover Frequencies of Neopentane Hydrogenolysis on Rh/Al_2O_3 and Rh/TiO_2 Thin Film Model Catalysts after Preoxidation at 723 K Followed by Low-Temperature Reduction at 523 K (LTR) and High-Temperature Reduction at 673 K (HTR)

	Turnover frequency (h^{-1})	
	LTR (523 K)	HTR (673 K)
7.8-nm Rh/Al_2O_3	90	18
7.8-nm Rh/TiO_2	150	<2
13.3-nm Rh/Al_2O_3	107	24
13.3-nm Rh/TiO_2	160	5

Note. Reaction conditions: 5 mbar neopentane; 100 mbar hydrogen; 900 mbar He. Reaction temperature: 473 K. Preoxidation at 723 K.

4. DISCUSSION

4.1. TEM Observations of Structural Changes

The micrographs in section 3 of this work, together with those of the previous papers (3, 5, 13), reveal clearly the structural and morphological changes of Rh nanocrystals upon oxidation and reduction. The results obtained so far are in good agreement with earlier observations on supported (model) catalysts, e.g., of Datye *et al.* (16, 23) and of Schmidt *et al.* (24, 25). Contrary to most of the previous studies, we limited the temperature of oxidation and reduction to 723 K, to simulate a "normal" catalyst activation and to avoid too extensive structural changes usually associated with SMSI.

Upon an oxidation up to 723 K, the observed structural changes, eventually resulting in particles surrounded by epitaxial oxide, were rather independent of the Rh particle size and the type of support. In summary, the effect of a consecutive reduction can be divided into four steps: (i) Reduction at 373–423 K removed the surface oxide. (ii) After reduction between 523 and 573 K, the majority of the particles exhibited irregular profiles (indicating small high-index facets) or polycrystalline shapes (with "rough" high-index surfaces). (iii) After reduction at 573 K and

above, the profiles of the particles appeared smoother, indicating larger and lower-index faces. (iv) Finally, reduction temperatures higher than 573 K led to coalescence of larger particles with small interparticle distances. The coalescence was induced by spreading of the Rh particles, i.e., by an increase in surface wetting, and it occurred more easily on titania (starting between 573 and 623 K) than on alumina (above 673 K). Although surface wetting phenomena are well known to occur upon reduction of small (1- to 3-nm range) noble-metal catalyst particles on various supports (see, e.g., the reviews by Ruckenstein and Dadyburjor (26) and by Bartholomew (27)), they have been usually observed after reduction at much higher temperature, i.e., 773 K and above. In those cases, the formation of two-dimensional "raftlike" Rh particles was also reported (28).

To understand the spreading of large particles upon reduction, we must distinguish between nonreducible and reducible supports. Nonreducible support materials are not chemically affected by a hydrogen treatment at or below 723 K. The extent of their interaction with the noble metal under the influence of hydrogen has been under debate for some time (29, 30). If we exclude surface alloy formation as the driving force for spreading under our experimental conditions, the lowering of the interfacial free energy may either result from the removal of hydroxyl groups from the alumina surface, or from the formation of defect centers at the surface (31) or, more likely, from the removal of the "hydrogen cushion" from the interface between particle and support by HTR (32–34). It is well-known from several examples that a further increase of the reduction temperature above 773 K would lead to wetting and coalescence on almost any oxidic support, usually under alloy formation, as has, e.g., recently been evidenced for Rh on SiO_2 (35).

On the contrary, the reduction of the surface of reducible supports induces the formation of oxygen vacancies and of lower-valent cations already at much lower temperature. The observed differences between supporting titania and supporting alumina may therefore be connected to the number of oxygen vacancies, and correspondingly of lower-valent Ti ions, created on the titania surface. Kramer *et al.* (36) have recently determined the number of surface oxygen vacancies arising from hydrogen reduction of titania powder under experimental conditions comparable to ours. For our case (reduction temperature, between 523 and 673 K; water vapour pressure in the circulation reactor, <1 mbar), their number can be estimated to range between 0.1 and 2% of the surface oxygen atoms. The oxygen vacancies may affect the interfacial energy between Rh metal and support and therefore induce wetting and spreading around 573 K.

A reverse effect, the migration of Ti suboxide species on top of the Rh metal particles upon high-temperature reduction (>773 K), also well-known as encapsulation or decoration, has been evidenced by high-resolution electron microscopy for some time (37–39) and was also claimed to be responsible for the SMSI behaviour of titania-supported Rh catalysts (18, 40, 41). More recently, Pesty *et al.* could show by X-ray photoelectron spectroscopy and low-energy ion scattering that encapsulation of Pt islands on rutile by migrating titanium suboxide species may already occur at much lower temperature, e.g., upon annealing in an ultra-high vacuum (uhv) above 450 K (42). In two recent STM studies, Berkó *et al.* (43, 44) obtained strong evidence for TiO_x encapsulation of Rh particles deposited onto TiO_2 single-crystal surfaces: On a TiO_2 (110)-(1×2) surface, they detected decoration of small Rh particles upon annealing in an uhv to 500–700 K (43), and on TiO_2 (110)-(1×1), they observed the encapsulation of small clusters and of large (10- to 15-nm) Rh particles induced by 10^{-4} mbar H_2 treatment at 750 K (44). Although so far HREM has revealed decorating titanium suboxide overlayers on Rh only after an extensive reduction at 773 K, it has to be kept in mind that an already existing "monolayer decoration" of Ti suboxide resulting from (lean) reduction at lower temperature may be easily reversed by the transfer of the sample into the electron microscope (generally through air). It is therefore conceivable that encapsulation connected with catalyst deactivation has occurred in previous experiments as well as on the present Rh/titania catalysts upon reduction at temperatures far below 773 K, even though it could not be detected *ex situ* in the electron microscope. Advances in HREM specimen handling (vacuum or controlled atmosphere transfer, low-temperature sample passivation, etc.) that become more and more routine will certainly contribute to answering this question.

4.2. Kinetics

It follows from the electron microscopic investigation that a reproducible reference state for kinetic measurements on "higher loading" catalysts can only be established after an activation cycle including an oxidation of *already coalesced* particles at 673–723 K, followed by LTR between 523 and 573 K. This results in particles like those depicted, e.g., in Fig. 5b for the 13.3-nm Rh/titania catalyst. After this pretreatment, the measured activities were reproducible within 20% after every consecutive cycle of HTR/O_x/LTR. As mentioned, the particle distribution in this case is bimodal and contains also small Rh particles (<2 nm) (20). However, due to their small number and very small surface area, their contribution to the overall activity can presumably be neglected. The fact that catalysts of smaller (7.8-nm) and of larger (13.3- and 16.7-nm) mean particle size differ in their catalytic behaviour is not surprising since the latter have undergone a complete restructuring of the particle surface and also of the metal–support boundary.

A comparison of the activity of the two 7.8-nm catalysts after LTR reveals that the presence of a *nonreduced*

(stochiometric) titania support promotes the hydrogenolysis of MCB on Rh particles. A 373 K reduction removes most of the Rh oxide but introduces only very few oxygen vacancies on the titania surface. After this treatment, the maximum activity is measured on titania while alumina-supported Rh particles show no activity. From the related methylcyclopentane (MCP) ring-opening reaction, we know that the ring-opening activity increases if we increase the acidity of the support (45, 46). We therefore tentatively attribute the strong promotion of the methylcyclobutane reaction to the acidity of *unreduced* titania.

After a 523 K reduction, the activity has reached a maximum on alumina, when particles still exhibit polycrystalline features and/or moderate surface faceting (3). This is in agreement with observations that particles with more disordered surface structures, as obtained, e.g., after oxidation, show higher activity in consecutive hydrogenolysis reactions (16, 47). On the contrary, after reduction at 523 K, Rh particles on titania have lost nearly 90% of their former activity. Finally, after a 723 K reduction, the activity of the titania-supported catalyst is almost negligible while the corresponding alumina-supported film has experienced only a small activity decrease. While the latter can again be quite well understood by considering the concomitant changes from more disordered surface structures (high-index facets) to less reactive low-index facets (48), there exist a number of possible explanations for the drastic activity loss of Rh/TiO_2 upon reduction at relatively low temperature. For the suppression of catalytic properties of supported noble metals upon HTR (773 K and above), two main mechanisms have been proposed some time ago (49): the decoration by migrating suboxide and a charge transfer between metal and support. From the previous discussion and from Refs. (42) and (43), we may deduce that encapsulation by TiO_x may already set in upon a reduction around 450 K and therefore cause deactivation at much lower temperature than previously expected. However, a reasonable explanation of the observed exponential activity decrease on *small* Rh particles on TiO_2 may also be given considering the increasing number of oxygen vacancies, and of lower-valent Ti cations, on the titania surface with increasing reduction temperature, as already mentioned in section 4.1. Kramer *et al.* (36) showed that the (equilibrium) number of oxygen vacancies on the titania surface increases exponentially with the reduction temperature in the range of interest between 323 and 673 K. The observed activity decrease can therefore also be seen in relation to an exponential increase of the number of Ti^{3+} sites on the surface. Following in principle the arguments given by Verykios *et al.* (50, 51), we may further argue that the promotion of a hydrogen–hydrocarbon reaction on Rh metal particles by *unreduced* titania may occur via a local electric field acting at the metal–oxide boundary. This field (Schottky barrier) arises from a (small) charge transfer between metal and support, compensating for the differences between the two Fermi levels, and it is stronger on a more acidic support (46, 52). The effect of this field will be reduced or even inverted by an increasing number of lower-valent Ti cations near the perimeter of the Rh particles (51), and this should lead to a parallel decrease of activity for hydrocarbon reactions, as actually observed. Sanz *et al.* (34) have suggested that hydrogen incorporated in the oxygen vacancies at the metal–support interface may also contribute by site blocking. Of course, at more elevated temperatures, the suboxide migration will play an additional role in further decreasing the activity. Altogether, the observed activity results from a superposition of three different phenomena: TiO_2 promotion after reduction at very low temperature and inhibition by Ti^{3+} formation and passivation by TiO_x overlayers, both increasing with increasing reduction temperature.

Furthermore, the structural changes observed on the 13.3- and 16.7-nm catalysts, containing larger and more densely packed Rh particles, may help to explain the different catalytic activity with respect to the 7.8-nm catalyst. Upon reduction, all three Al_2O_3-supported Rh catalysts behave similarly, but the activity decrease upon LTR (373–473 K) of the 13.3- and 16.7-nm Rh/TiO_2 catalysts is less pronounced than that of the 7.8-nm Rh/TiO_2 sample. Here, we have to take into account the relative dimensions of metal and supporting oxide in the different catalyst systems. If spreading and coalescence have resulted in very large Rh particles, the number of Ti^{3+} sites created at the interface by partial reduction of the support may not be sufficient to induce dramatic activity changes. In addition, a beginning surface decoration will affect larger particles less than smaller ones. Only after longer reduction at higher temperature will the combined effects of oxygen-vacancy formation and of suboxide migration lead to the observed rapid decrease of reaction rates, until they almost diminish after reduction at 723 K.

In each case, the deactivation of Rh on titania and on alumina could be fully reversed by oxidation at 673 K and by subsequent reduction at 373 and 523 K, respectively. Also, subsequent oxidation/reduction cycles yielded reproducible ring-opening activities, reminiscent of the "oscillatory" behaviour observed by Logan *et al.* (16) and by Schmidt *et al.* (47) in alkane hydrogenolysis on Rh particles on SiO_2 supports and on Rh single crystals within cycles of oxidation and low- and high-temperature reduction.

It is also worthwile to compare our findings with the ring-opening activities in the related reaction of methylcyclopentane (MCP) on Rh/TiO_2, in particular, with the results obtained by Fenoglio *et al.* (53) after oxidation at 673 K and consecutive reduction between 423 and 773 K. They report that the turnover rates for all three products (3-methylpentane, 2-methylpentane, and *n*-hexane) pass a maximum after reduction at 550 K and decrease strongly

upon further reduction. They suggest that after reduction at 550 K an optimal surface configuration is obtained. In addition, the selectivity (the ratio between *n*-hexane and branched hexanes; minimum at about 550 K) varies considerably with the reduction temperature, suggesting either a change in ensemble size, as Resasco *et al.* believe, or a changing contribution from the metal–oxide boundary to the overall reaction (46).

Finally, it should be mentioned that the initial rates of the neopentane conversion measured after LTR and HTR follow the same general trend as those of the MCB ring-opening reaction: Titania-supported Rh has its maximum activity at the lowest possible reduction temperature, i.e., 473 K (not shown in the table), and the activity decreases with T_{red}, similar to that in the MCB reaction. Rh/Al_2O_3 has an activity maximum after 523 K reduction, followed also by a moderate decrease. This general trend agrees well with previous observations on Rh powders and evaporated films by Karpinski *et al.* (22), whereas the stronger influence of the support on the MCB reaction is probably due to a different reaction mechanism.

5. CONCLUSIONS

The following conclusions can be drawn from the present study: Epitaxially grown noble-metal nanoparticles on oxidic supports are well-suited models to monitor structural and morphological changes during oxidation and low- and high-temperature reduction. Electron microscopy revealed that a hydrogen reduction at 723 K caused support wetting and spreading of large (>10 nm) and closely spaced Rh nanocrystals on alumina, while on titania the same effect occurs already upon reduction at 623 K. The different behaviours are attributed to a change in the interfacial energy between Rh and titania as a result of the formation of oxygen vacancies on the titania surface upon reduction. On either support, the Rh catalyst particles undergo drastic changes of morphology and surface area during every cycle of high-temperature reduction, oxidation, and low-temperature reduction, but end up every time in a reproducible state.

Measurements of the catalytic activity in the ring-opening reaction of methylcyclobutane, performed parallel to the electron microscopic investigation, revealed pronounced differences in the catalytic behaviour of identical Rh nanoparticles on titania and on alumina. These can only in part be related to the microstructure of the particles (e.g., surface roughness, size, shape, etc.). It is suggested that the activity decrease of titania-supported rhodium with increasing reduction temperature is due to a superposition of two effects: Changes of the electric field at the metal–support boundary with increasing number of low-valent Ti cations on the surface and increasing decoration (encapsulation) of the metal particles by migrating Ti suboxide.

ACKNOWLEDGMENTS

Part of this work was supported by the Fonds zur Förderung wissenschaftlicher Forschung of Austria (Projects 8719 and S-8105). We also thank Reinhard Kramer for helpful discussions.

REFERENCES

1. Tauster, S. J., and Fung, S. C., *J. Catal.* **55**, 29 (1978).
2. Haller, G. L., and Resasco, D. E., *Adv. Catal.* **36**, 173 (1989).
3. Rupprechter, G., Hayek, K., and Hofmeister, H., *J. Catal.* **173**, 409 (1998).
4. Rupprechter, G., Hayek, K., and Hofmeister, H., *Nanostruct. Mater.* **9**, 311 (1997).
5. Rupprechter, G., Hayek, K., Rendón, L., and José-Yacamán, M., *Thin Solid Films* **260**, 148 (1995).
6. Rupprechter, G., Seeber, G., Hayek, K., and Hofmeister, H., *Phys. Status Solidi A* **146**, 449 (1994).
7. Hayek, K., *J. Mol. Catal.* **51**, 347 (1989).
8. Zimmermann, C., and Hayek, K., *Chem. Ing. Tech.* **63**, 68 (1991).
9. Bartók, M., Török, B., Molnár, A., and Apjok, J., *React. Kinet. Catal. Lett.* **49**, 111 (1993).
10. Zimmermann, C., and Hayek, K., *in* "New Frontiers in Catalysis, Proceedings, 10th International Congress on Catalysis, Budapest, 1992" (L. Guczi, F. Solymosi, and P. Tetenyl, Eds.), p. 2375. Elsevier, Budapest, 1993.
11. Török, B., and Bartók, M., *Catal. Lett.* **27**, 281 (1994).
12. Török, B., Palinko, I., Molnár, A., and Bartók, M., *J. Catal.* **159**, 500 (1996).
13. Rupprechter, G., Hayek, K., and Hofmeister, H., *Vacuum* **46**, 1035 (1995).
14. José-Yacamán, M., and Avalos-Borja, M., *Catal. Rev.-Sci. Eng.* **34**, 55 (1992).
15. Henry, C. R., Chapon, C., Duriez, C., and Giorgio, S., *Surf. Sci.* **253**, 177 (1991).
16. Logan, A. D., Sharoudi, K. A., and Datye, A. K., *J. Phys. Chem.* **95**, 5568 (1991).
17. Kalakkad, D., Anderson, S. L., Logan, A. D., Pena, J., Braunschweig, E. J., Peden, C. H. F., and Datye, A. K., *J. Phys. Chem.* **97**, 1437 (1993).
18. Bernal, S., Botana, F. J., Calvino, J. J., Lopez, C., Perez-Omil, J. A., and Rodríguez-Izquierdo, J. M., *J. Chem. Soc., Faraday Trans.* **92**, 2799 (1996).
19. Datye, A. K., and Smith, D. J., *Catal. Rev.-Sci. Eng.* **34**, 129 (1992).
20. Wang, T., and Schmidt, L. D., *J. Catal.* **70**, 187 (1981).
21. Sárkány, A., Matusek, K., and Tétényi, P., *J. Chem. Soc., Faraday Trans.* **73**, 1699 (1977).
22. Karpinski, Z., Juszczyk, W., and Pielaszek, J., *J. Chem. Soc., Faraday Trans.* **83**, 1293 (1987).
23. Chacraborti, S., Datye, A. K., and Long, N. J., *J. Catal.* **108**, 444 (1987).
24. Gao, S., and Schmidt, L. D., *J. Catal.* **111**, 210 (1988).
25. Burkhardt, J., and Schmidt, L. D., *J. Catal.* **116**, 240 (1989).
26. Ruckenstein, E., and Dadyburjor, D. B., *Rev. Chem. Eng.* **1**, 251 (1983).
27. Bartholomew, C. H., *in* "Catalysis," Vol. 10, p. 41. The Royal Society of Chemistry, Cambridge, 1993.
28. Yates, D. J. C., Murrell, L. L., and Prestridge, E. B., *J. Catal.* **57**, 41 (1979).
29. Yao, H. C., and Shelef, M., *J. Catal.* **56**, 12 (1979).
30. Yao, H. C., Gandhi, H. S., and Shelef, M., *Stud. Surf. Sci. Catal.* **11**, 159 (1982).
31. Duprez, D., Sadi, F., Miloudi, A., and Percheron-Guégan, A., *Stud. Surf. Sci. Catal.* **71**, 629 (1991).
32. Vaarkamp, M., Modica, F. S., Miller, J. T., and Koningsberger, D. C., *J. Catal.* **144**, 611 (1993).

33. Vaarkamp, M., Miller, J. T., Modica, F. S., and Koningsberger, D. C., *J. Catal.* **163**, 294 (1996).
34. Belzunegui, J. P., Sanz, J., and Rojo, J. M., *J. Am. Chem. Soc.* **114**, 6749 (1992).
35. Sadi, F., Duprez, D., Gérard, F., Rossignol, S., and Miloudi, A., *Catal. Lett.* **44**, 221 (1997).
36. Haerudin, H., Bertel, S., and Kramer, R., *J. Chem. Soc., Faraday Trans.* **94**, 1481 (1998).
37. Singh, A. K., Pande, N. K., and Bell, A. T., *J. Catal.* **94**, 422 (1985).
38. Bernal, S., Calvino, J. J., Cauqui, M. A., Cifredo, G. A., Jobacho, A., and Rodríguez-Izquierdo, J. M., *Appl. Catal. A* **99**, 1 (1993).
39. Bernal, S., Calvino, J. J., López-Cartes, C., Pintado, J. M., Pérez-Omil, J. A., Rodríguez-Izquierdo, J. M., Hayek, K., and Rupprechter, G., *Catal. Today* **52**, 29 (1999).
40. Sadeghi, H. R., and Henrich, V. E., *J. Catal.* **87**, 279 (1984).
41. Braunschweig, E. J., Logan, A. D., Datye, A. K., and Smith, D. J., *J. Catal.* **118**, 227 (1989).
42. Pesty, F., Steinrück, H. P., and Madey, T. E., *Surf. Sci.* **339**, 83 (1995).
43. Berkó, A., Ménesi, G., and Solymosi, F., *Surf. Sci.* **372**, 202 (1997).
44. Berkó, A., Ulrych, I., and Prince, K. C., *J. Phys. Chem. B* **102**, 3379 (1998).
45. Kramer, R., and Zuegg, H., *in* "Proceedings, 8th International Congress on Catalysis, Berlin, 1984" (G. Ertl, Ed.), Vol. 5, p. 275. VCH Weinheim, Berlin, 1984.
46. Hayek, K., Kramer, R., and Paál, Z., *Appl. Catal. A* **162**, 1 (1997).
47. Schmidt, L. D., and Krause, K. R., *Catal. Today* **12**, 1035 (1992).
48. Somorjai, G. A., and Rupprechter, G., *J. Chem. Educ.* **75**, 161 (1998).
49. Tauster, S. J., *in* "Strong Metal–Support Interactions" (R. T. K. Baker, S. J. Tauster, and J. A. Dumesic, Eds.), p. 1. ACS, Washington, DC, 1986.
50. Akubuiro, E. C., and Verykios, X. E., *J. Catal.* **113**, 106 (1988).
51. Ioannides, T., and Verykios, X. E., *J. Catal.* **161**, 560 (1996).
52. Kramer, R., and Fischbacher, M., *J. Mol. Catal.* **51**, 247 (1989).
53. Fenoglio, R. J., Nunez, G. M., and Resasco, D. E., *J. Catal.* **121**, 77 (1990).